Materials Advances

ROYAL SOCIETY OF CHEMISTRY

PAPER

View Article Online
View Journal | View Issue

Cite this: *Mater. Adv.*, 2026, 7, 425

Synergistic electrochemical detection of ciprofloxacin using bismuth vanadate nanocomposite-modified activated carbon derived from banana peel biomass

N. Mekgoe,*[a] N. Mabuba,[ab] D. Nkosi[ab] and K. Pillay[a]

Received 21st February 2025,
Accepted 2nd September 2025

DOI: 10.1039/d5ma00168d

rsc.li/materials-advances

Ciprofloxacin (CPX) is a persistent antibiotic pollutant that poses significant environmental challenges, requiring innovative detection methods. This study developed a novel nanocomposite sensor using activated carbon from banana peels (ACBP) modified with bismuth vanadate ($BiVO_4$) for electrochemical detection of CPX. Using advanced characterization techniques and differential pulse voltammetry (DPV), researchers demonstrated an excellent electrode performance with a detection range of 0.1–1 μM and remarkable accuracy, achieving a 99 ± 6% recovery rate in wastewater samples. The research highlights the potential of combining agricultural waste and nanomaterials to create sustainable environmental monitoring technologies, offering a promising, rapid, and cost-effective alternative to traditional detection methods like high-performance liquid chromatography and mass spectrometry.

Introduction

Ciprofloxacin (CPX) is a stable compound that can enhance the growth of toxic bacteria in freshwater and wastewater systems.[1] This antibiotic is a second-generation fluoroquinolone that is widely used in both agricultural settings and healthcare to treat bacterial infections in livestock and humans, effectively targeting both Gram-positive and Gram-negative bacteria.[2] Due to its widespread use and stable nature, ciprofloxacin is frequently detected in the environment worldwide.[3] Numerous antibiotics are expelled from living organisms through urine and faeces, leading to contamination of soil and water, which in turn contributes to the rapid spread of drug resistance.[4]

The majority of antibiotics are not completely metabolized and are commonly found at relatively high levels in soil, liquid manure, and surface waters, which are significantly affected by domestic wastewater and agricultural runoff. The inadequate regulation of antibiotic disposal on local and global scales has led to their long-term persistence in the environment.[5] This ongoing presence of antibiotics has led to the development of antibiotic-resistant genes in various pathogenic bacteria, which can infiltrate the food chain and present significant health risks to humans and other organisms. These risks include serious conditions such as heart disease, nervous system damage, and impaired blood circulation.[2,6]

Various techniques have been established for detecting CPX, such as high-performance liquid chromatography, mass spectrometry, spectrophotometry, and electrochemical methods.[7] However, many traditional approaches for CPX detection tend to be time-consuming and require expensive equipment. Additionally, there has been limited research focused on the electrochemical analysis of CPX.[8–10]

Despite extensive efforts to improve analytical approaches for quantitative and qualitative antibiotic detection, many conventional methods struggle to eliminate micro-pollutants like antibiotics due to their inability to detect trace levels, resulting in continuous discharge into water bodies. Therefore, there is a pressing need for complementary methods that are low-cost, feasible, and time-saving for antibiotic detection. Very few studies involving the electrochemical determination of CPX have been reported.[11]

Antibiotic detection has focused a lot of interest on electrochemical detection methods because of their low cost, easy online monitoring, quick response, high sensitivity, and ease of us. The electrocatalytic activity of the working electrode plays a major role in the efficacy of electrochemical sensors. Therefore, a key factor in these sensors' performance is the design of the electrode materials.[12] The electrode surface must be modified with the right functional materials in order to enhance the electrochemical signal and response time in these sensors.[13,14]

In electrochemical detection analysis, choosing the right sensing material is essential.[15] In particular, substances that

[a] *Faculty of Science, Department of Chemical Sciences, University of Johannesburg, No. 1, cnr. Nindt and Beit Street, Doornfontein, 2028, Republic of South Africa. E-mail: kriveshinip@uj.ac.za*
[b] *Centre of Nanomaterials Science Research, University of Johannesburg, Department of Chemical Sciences, No. 1, cnr. Nindt and Beit Street, Doornfontein, 2028, Republic of South Africa*

exhibit several oxidation states can offer an abundance of active sites for interacting with the target analyte.[16] $BiVO_4$ and vanadium oxide offer several advantages for enhancing the efficacy of electrochemical sensors that are employed in ciprofloxacin detection. But pure vanadium oxide is less electrically conductive, which might make it less useful in these sensors.[17,18] To tackle this issue, researchers have implemented strategies to improve electrical and ionic conductivity, as well as redox chemistry, by doping with various transition metal oxides, hydroxides, and carbon-based materials.[18,19]

Vanadium oxide exhibits many oxidation states (+2, +3, +4, and +5) which provides numerous active sites for interaction with ciprofloxacin, enhances the electronic structure of its products, and has gained attention due to its physicochemical characteristics and excellent stability.[17,18] $BiVO_4$ enables rapid electron transport for the electrochemical sensor, provides superior cycling stability, and offers selectivity towards ciprofloxacin as the target analyte.[18] While vanadium oxide has advantages, its low electrical conductivity might hinder the performance of electrochemical sensors. To improve conductivity and redox characteristics, doping with other materials is necessary, which complicates the process of fabricating sensors.[20] Electrochemical sensors still struggle to eliminate ciprofloxacin micropollutants at trace levels, resulting in continuous discharge into water bodies, and more research is needed to develop complementary methods that are low-cost, feasible, and time-saving for antibiotic.[21]

Bimetallic nanocomposites have garnered significant attention in electrochemistry due to their enhanced catalytic activity compared to their monometallic counterparts. This enhanced activity arises from synergistic effects between the two metals, which can modify the electronic structure, increase the number of active sites, and facilitate improved charge transfer kinetics. For instance, the combination of a highly conductive material with a redox-active metal oxide can lead to significant improvements in sensor performance, as seen in the development of $BiVO_4$-based sensors where doping with transition metal oxides enhances electrical conductivity and redox chemistry. These synergistic effects make bimetallic nanocomposites promising candidates for enhancing the sensitivity and selectivity of electrochemical sensors for various analytes, including antibiotics like ciprofloxacin.[22]

In electrochemical sensors, pure vanadium oxide has a reduced electrical conductivity. In order to overcome these constraints, scientists have used methods such as doping with other transition metal oxides or hydroxides (such as nickel hydroxide, manganese dioxide, iron(III) oxide, cerium(IV) oxide, nickel oxide, ruthenium(IV) oxide, tin(IV) oxide, cobalt(II,III) oxide, titanium(IV) oxide, bismuth vanadate, and cobalt(II) hydroxide) and carbon-based materials like graphene, activated carbon, and single-walled carbon nanotubes (SWCNT) to overcome these limitations.[23–25] These materials offer several advantages, including high surface area, improved charge transfer rates, and increased catalytic activity, which contribute to enhanced sensitivity and selectivity in detecting analytes like ciprofloxacin.[26,27] For instance, graphene and carbon nanotubes are known for their excellent electrical conductivity and large surface area, allowing for greater interaction with the target analyte, thus improving sensor performance.[26,28] However, there are also disadvantages associated with these materials.[28] For example, while vanadium oxide provides multiple oxidation states beneficial for electrochemical reactions, its lower electrical conductivity can limit sensor performance, necessitating doping with other materials to overcome this limitation.[28,29] The complexity of sensor fabrication increases with the incorporation of multiple materials, which can lead to challenges in reproducibility and stability of the sensors over time.[26,27,30] While these doping strategies significantly enhance the performance of electrochemical sensors, they also introduce complexities that require careful consideration in sensor design and application.[27,31]

A tropical fruit that is extensively grown and eaten worldwide is the banana. The plentiful agricultural waste that comes from banana trees has attracted attention lately because of its possible uses in treating wastewater that contains heavy metals, dyes, and other organic contaminants. Activated carbon will be synthesized from banana peels[7,32] Given the significant impact of antibiotics in the environment and the potential applications of $BiVO_4$ and activated carbon from banana peels (ACBP), this study reports the synthesis of ACBP, which was subsequently used in the construction of photoanodes.[33]

Integrating $BiVO_4$ into ACBP significantly boosts the material's surface area and sensitivity, as well as increases its porosity, thus enhancing the efficiency of electrochemical analysis. Like other inorganic negative electrode materials, embedding bismuth vanadate within the carbon matrix is anticipated to improve particle electrical contact and enhance both cycling stability and rate performance.[34] This study introduces a novel nanocomposite sensor for ciprofloxacin (CPX) detection, leveraging activated carbon derived from banana peels (ACBP) modified with bismuth vanadate ($BiVO_4$). The innovation lies in the synergistic use of a sustainable, low-cost material (ACBP) with $BiVO_4$ to create a sensor that achieves a detection range of 0.1–1 μM and a 99 ± 6% recovery rate in wastewater samples, offering a promising, rapid, and cost-effective alternative to traditional methods. The proposed device was employed for detection of CPX from different types of water.

Materials

Banana peels were purchased from a local market in South Africa. All chemical reagents used in the experiments were of analytical grade and obtained from Sigma Aldrich, South Africa. These included potassium hydroxide (85%), ethylene glycol ($C_2H_6O_2$, 99.8%), hydrochloric acid (37%, diluted to 1.0 M HCl), sodium hydroxide (NaOH, 98%), ethanol (99.8%), bismuth(III) nitrate ($Bi(NO_3)_3{\cdot}5H_2O$, ≥98.0%), vanadium(IV) oxide sulfate ($VOSO_4{\cdot}xH_2O$, 97%), monopotassium phosphate (KH_2PO_4), dipotassium phosphate (K_2HPO_4), nitric acid (HNO_3, >68.0%), potassium hydroxide (KOH, pellets), and sodium acetate (CH_3COONa, >99.0%). All chemicals were used without

any further treatment. Throughout the experiments, deionized water prepared by (Brand, Country of purchase) was utilized.

Apparatus

Micrographs of both unmodified and nano-modified electrodes were captured using a field emission scanning electron microscope (FESEM), specifically the Zeiss Crossbeam 540 FEG SEM, which is equipped with an Oxford Instruments energy dispersive X-ray spectrophotometer (EDS) detector located in the United Kingdom. All electrochemical experiments were conducted using an Ivium Compactstat potentiostat from the Netherlands in a three-electrode setup, consisting of a platinum wire as the counter electrode, a glassy carbon working electrode, and an Ag/AgCl (3 M KCl) reference electrode. For electrochemical impedance spectroscopy (EIS), a bias potential of 0.22 V was applied over a frequency range from 100 kHz to 100 mHz. The conditions for cyclic voltammetry included a potential range of −0.2 V to 1.0 V, an E-step of 0.03 V, a current range of 1 μA, and a scan rate of 50 mV s^{-1} in a ferro/ferricyanide solution. Validation studies were performed using square wave voltammetry and UV-visible spectrometry with a Thermo Fisher ICAP6500 Duo instrument sourced from China. All electrochemical measurements were carried out at room temperature (25 °C).

Preparation of activated carbon banana peels (ACBP)

The banana peels (BP) were dried at 60 °C for 24 hours after being properly cleaned many times with distilled water and acetone to remove any remaining dirt. Following cleaning and drying, 10 g of the raw material was steeped in a solution containing 10 mL of 0.5 M sulfuric acid and 100 mL of distilled water. The peels were then chopped into smaller pieces. Then, this combination was put into a 120 mL autoclave made of stainless steel, sealed, and heated to 160 °C for 12 hours. The finished black carbon was filtered and dried at 80 °C for 48 hours after being permitted to naturally cool to room temperature. Using an agate mortar, the dried carbon was mixed with potassium hydroxide pellets in a 1 : 1 mass ratio. It was then cautiously moved to a horizontal tube furnace for carbonization, or activation. For one hour, argon gas was continuously supplied during the carbonization process, which involved heating the material at a rate of 5 °C per minute to 800 °C. After that, the activated carbon was cleaned till a pH of neutral using distilled water and 3 M hydrochloric acid. Afterwards, the samples were given the ACBP designation after the activated carbon was dried in an electric oven for 24 hours at 60 °C. Scheme 1 provides a schematic diagram showing the synthesis of ACBP.

Scheme 1 Schematic diagram of the synthesis of activated carbon banana peels (ACBP).

Synthesis of bismuth vanadate nanostructures

Bismuth nitrate pentahydrate (2 g) and 0.8 g of citric acid (as a chelating agent) were dissolved in 10 mL of ethylene glycol with vigorous stirring to form solution A, which was the precursor to bismuth vanadate nanostructures. Solution B was made in the meantime by dissolving 0.5 g of ammonium vanadate in 25 mL of deionized water. After adding solution B to solution A dropwise, 30 mL of ethanol was added and stirred constantly for 30 minutes. After the mixture was homogenous, 0.85 g of sodium carbonate was added to change the pH. The resultant solution was hydrothermally treated for 24 hours at 180 °C in a steel autoclave lined with Teflon. Following the treatment, the precipitates were allowed to cool before being cleaned with deionized water and 100% ethanol and dried for six hours at 80 °C. For five hours, the calcination process was carried out at 400 °C.[35] This was labelled $BiVO_4$.

Fabrication of cellulose-supported bismuth vanadate nanocomposites

Activated carbon banana peel-supported bismuth vanadate (ACBP/$BiVO_4$) nanocomposites were developed by incorporating varying weight ratios of 50 mg of ACBP during the initial step of dissolving bismuth nitrate. Solution B was prepared in a similar manner and subsequently added to solution A. The resulting solutions were stirred and placed in a Teflon-lined steel autoclave at 180 °C for 24 hours. Following this, green precipitates were collected, cooled, and subjected to centrifugation (5000 rpm, room temperature) for 10 minutes. The precipitate was washed twice with deionized water and ethanol, then dried at 60 °C for 24 hours, and labelled ACBP–$BiVO_4$. A schematic diagram illustrating the synthesis process of ACBP–$BiVO_4$ is presented in Scheme 2.

Preparation and electrochemical characterisation of the modified GCE

Bare glassy carbon electrodes (GCEs) were cleaned by polishing with alumina powders of different sizes (0.3, 0.05, and 0.01) on

Scheme 2 Schematic diagram of the synthesis of activated carbon bismuth vanadate (ACBP–$BiVO_4$).

polishing pads, followed by rinsing with deionized water and sonicating in a 1 : 1 mixture of deionized water and ethanol for five minutes. After the cleaning process, the electrodes were activated through cyclic voltammetry within a potential range of −0.2 V to 0.7 V in a 0.1 M phosphate buffer solution (PBS) at pH 7, using a scan rate of 50 mV s^{-1}.

Next, the GCE was modified with a composite of activated carbon from banana peels and bismuth vanadate (ACBP–$BiVO_4$). To prepare this, 10 mg of ACBP–$BiVO_4$ was measured and placed in a flask, followed by the addition of 5 mL of *N*,*N*-dimethylformamide (DMF) and 5 mL of 5 wt% Nafion (the binder). The mixture was sonicated for 30 minutes at 50 kHz to create a stable and homogeneous dispersion at a concentration of 1 mg mL^{-1}. This suspension was then applied to the working electrode of the GCE using a drop-casting technique, with a total volume of 6 μL applied in three separate 2 μL increments. The solution was allowed to evaporate at room temperature, as depicted in Scheme 1. The modified electrode was labeled as ACBP–$BiVO_4$.

The same procedure was followed for the individual modification of ACBP and $BiVO_4$ electrodes. The modified electrodes underwent cyclic voltammetry for 5 scans to reactivate them in 0.1 M PBS within a potential range of −0.2 to +0.7 V at a scan rate of 50 mV s^{-1}.

Scheme 3 demonstrates the drop-casting method used for depositing the nanomaterial onto the GCE. The oxidation mechanism indicates that the analyte, CPX, will experience electro-oxidation, and the secondary amine group may be oxidized to hydroxylamine derivatives, due to the presence of a secondary amino group, which acts as a strong electron-accepting group, as illustrated in Scheme 3. This detection principle underpins the analysis of CPX using the modified electrode.

To detect ciprofloxacin, cyclic voltammetry (CV) measurements were carried out in a static phosphate buffer solution (PBS) at pH 7, employing a scan rate of 50 mV s^{-1} and a potential range from −0.2 to 0.8 V. In addition, differential pulse voltammetry (DPV) was executed with the following settings: a starting potential of −1.6 V, an ending potential of 1.3 V, a pulse amplitude of 50.0 mV, a potential step of 4 mV, a pulse duration of 10 ms, a scan rate of 100 mV s^{-1}, and an equilibrium time of 5 seconds.

Modification of ACBP–$BiVO_4$ on the GCE surface

To begin, the purchased graphitic carbon electrode (GCE) was rinsed with distilled water and ethanol to eliminate impurities. Subsequently, 0.005 g of $BiVO_4$ was dissolved in 1 mL of deionized water and sonicated for 15 minutes to achieve a uniform electrocatalyst suspension. An optimized volume of 8 μL of this $BiVO_4$ slurry was then drop-coated onto the SPCE and dried at 50 °C. The modified electrode was subsequently used for various electrochemical studies, including electrode impedance spectroscopy (EIS), cyclic voltammetry (CV), and differential pulse voltammetry (DPV) analysis.

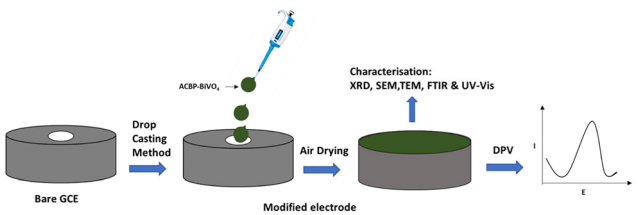

Scheme 3 Modification of GCE electrode with ACBP–$BiVO_4$ by drop casting method.

Preparation of real samples

Sample preparation and pre-treatment

Wastewater samples are collected from the intended source. To remove particulate matter that could interfere with the electrochemical measurements, the samples undergo filtration. The wastewater was filtered using a 0.45 μm pore size. Upon collection, measurements of the wastewater were taken for temperature (20.2 °C) and pH (7.14 ± 0.09), each parameter being measured three times for consistency. The next step, researchers typically adjust the sample pH to match that of the phosphate buffer solution (PBS) electrolyte. This ensures consistency during electrochemical analysis.

Spiking and electrochemical measurement

To evaluate the sensor's accuracy and recovery in the wastewater matrix, the filtered wastewater samples are spiked with known concentrations of ciprofloxacin (CPX). A stock solution of CPX is prepared, and appropriate volumes are added to the wastewater to achieve the desired concentrations. Differential pulse voltammetry (DPV) is then performed using a three-electrode system, with the modified GCE/ACBP–$BiVO_4$ electrode as the working electrode, a platinum wire as the counter electrode, and an Ag/AgCl reference electrode. DPV parameters are optimized for CPX detection and the same parameters are used for the real water samples.

Data analysis and validation

The peak current for CPX oxidation is obtained from the DPV voltammograms. A previously established calibration curve (peak current *vs.* CPX concentration) with standard CPX solutions in PBS is used to determine the CPX concentration in the wastewater samples. The recovery rate for the spiked samples is calculated to validate the accuracy of the method. Optional interference studies can be performed by adding common interferents found in wastewater to assess the sensor's selectivity. This detailed procedure ensures a comprehensive evaluation of the ACBP–$BiVO_4$ nanocomposite sensor for CPX detection in real-world wastewater samples.

Experimental

Results and discussion

The FTIR spectra for the samples $BiVO_4$, ACBP, and ACBP–$BiVO_4$ are illustrated in Fig. 1. A stretching frequency at 3455 cm^{-1} was observed in $BiVO_4$, ACBP, and ACBP–$BiVO_4$, attributed to the O–H group from carboxylic acids or alcohols.[36,37] The band at

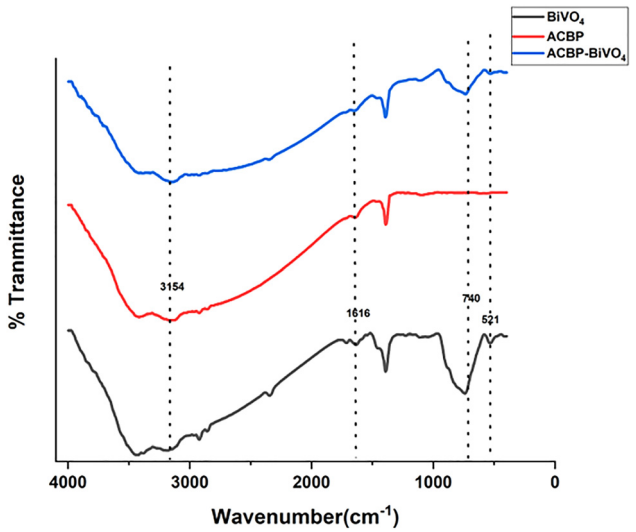

Fig. 1 (a) FTIR spectra of $BiVO_4$, ACBP and ACBP–$BiVO_4$.

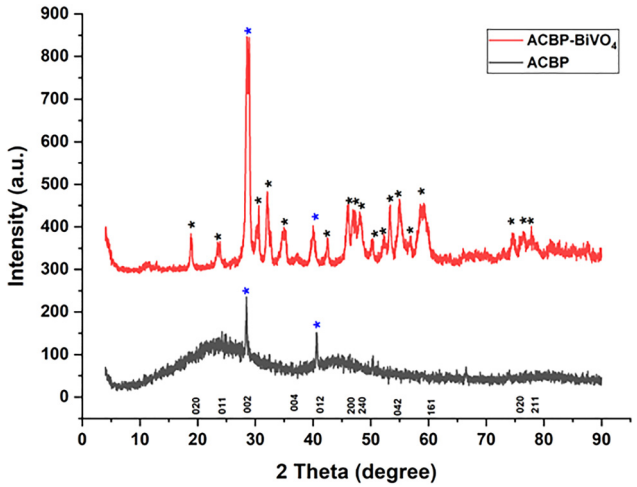

Fig. 2 XRD patterns of the prepared ACBP and ACBP–$BiVO_4$.

1616 cm^{-1} corresponds to aromatic C═C, confirming the presence of carbon bonds within the composite.[37,38] Additionally, the stretch at 1393 cm^{-1} is linked to C–O–C bonds. The absorption band found between 700 and 900 cm^{-1} relates to the symmetric and asymmetric stretching vibrations of the VO^- bond.[21] Various $BiVO_4$ molecules exhibit pronounced and broad absorption bands at 736 cm^{-1}, which are associated with VO_4^{3-} asymmetric stretching, while the 828 cm^{-1} band correlates with VO_4^{3-} symmetrical stretching, suggesting alterations in particle size and variations in the metal–oxygen bond distances among the $BiVO_4$ molecules. The Bi–O vibration exhibits a consistent shape and position at the absorption band of 533 cm^{-1}, but the 736 cm^{-1} band, related to VO^- vibration, shows a significant upward shift. This indicates potential structural changes within the VO_4^{3-} tetrahedron, which may be responsible for the 740 cm^{-1} peak stemming from the υ^3 asymmetric stretching vibration of VO_4.[39]

Fig. 2 presents the XRD patterns of the samples. The ACBP show a broad peak at 28.44° and 40.54°. These peaks can be assigned to the planes (002) and (012) associated with the reflection of graphite,[38] ACBP–$BiVO_4$ shows a distinct peaks at 18.77°; 23.46°; 28.54°; 30.58°; 32.01°; 34.66°; 39.66°; 39.98°; 42.48°; 45.93°; 53.98°; 54.85° and 59.17° which corresponds monoclinic scheelite phase indexed (020), (002), (121), (040), (200), (150), (240), (042), (202) and (161) corresponding to JCPDS-01-83-1699 some high peaks and low peaks indicate discrepancies in its crystallinities.[40] The highest intensity to the monoclinic phase at 28.90° which can be interfered to the monoclinic phase of $BiVO_4$. Lattice constants were found to be a = 5195 Å, b = 1170 Å and c = 5029 Å.[41]

The microstructural and morphological properties of $BiVO_4$ were investigated using field emission scanning electron microscopy (FE-SEM), energy-dispersive X-ray spectroscopy (EDX), and transmission electron microscopy (TEM). The FE-SEM images presented in Fig. 3(a) illustrate the interconnected microporous architecture of activated carbon derived from banana peel (ACBP). The activating agent employed during the carbonization process functions as a dehydration agent, facilitating the charring and aromatization of carbon, which subsequently leads to pore formation. The porous and defective characteristics of the synthesized ACBP can be attributed to the elimination of hydrogen, oxygen, and nitrogen (non-carbon elements) during carbonization. This release of elements from the char surface likely contributes to the development of a rigid carbon framework with a rudimentary pore structure. Fig. 3(b) depicts $BiVO_4$, which exhibits a sheet-like hierarchical morphology, while Fig. 3(c) shows that the synthesized ACBP–$BiVO_4$ also possesses a similar sheet structure. This configuration is hypothesized to provide a higher surface area compared to ACBP and $BiVO_4$ alone. Fig. 3(d) presents the elemental composition of $BiVO_4$, with the EDX profile confirming the presence of carbon (C), bismuth (Bi), vanadium (V), and oxygen (O) in the following respective percentages: 17.02%, 27.62%, 3.80%, and 66.47%, thereby validating the formation of $BiVO_4$.

Fig. 4a and b present varying magnifications of the ACBP–$BiVO_4$ composite, revealing two distinct types of ultrathin structures within the field of view. The dark, flat sheets exhibiting a regular morphology correspond to $BiVO_4$, while the bright,

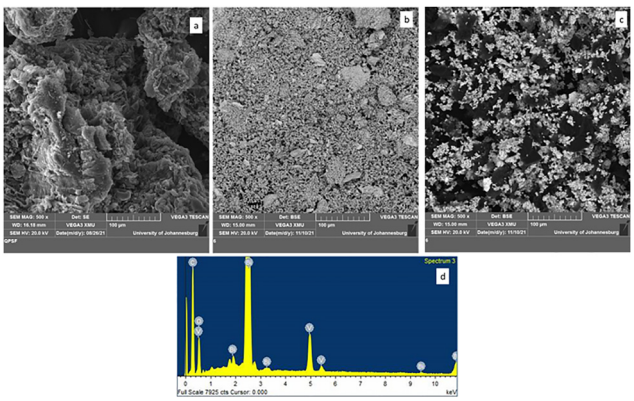

Fig. 3 SEM images of (a) ACBP and (b) $BiVO_4$, (c) ACBP/$BiVO_4$ and (d) EDS spectrum for the elemetal composition.

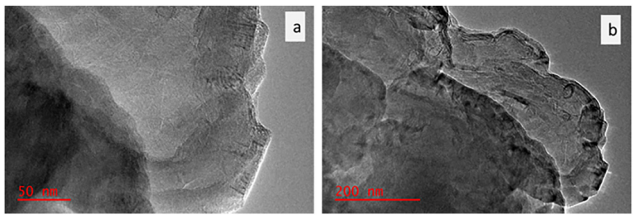

Fig. 4 TEM images of (a) and (b) ACBP–$BiVO_4$.

crumpled sheets represent ACBP, which is consistent with the findings from the scanning electron microscopy (SEM) analysis. Moreover, the images demonstrate that $BiVO_4$ and ACBP are in close proximity, exhibiting strong interfacial contact. Additionally, the bismuth (Bi) nanoparticles are uniformly distributed across the surfaces and interfaces of both materials, indicating effective integration within the composite structure.

Electrochemical characterization of GCE and GCE/ACBP–$BiVO_4$

Randles–Sevcik eqn (1), the electroactive surface area (ESA) of the GCE and the ACBP–$BiVO_4$ modified GCE was calculated. Electrochemical impedance spectroscopy (EIS) is a powerful electrochemical technique employed to assess the electrical conductivity of various electrode materials. This method yields comprehensive insights into parameters such as the diffusion coefficient, solution resistance, and charge transfer resistance at the electrode/electrolyte interfaces. The charge transfer resistance (R_{ct}) is directly correlated with the radius of the semicircle observed in the EIS data. As illustrated in Fig. 5(a), the Nyquist plot for different materials modified on glassy carbon electrodes (GCE) in a 5 mM $Fe(CN)_6^{3-/4-}$ solution, within a frequency range of 0.1 Hz to 100 kHz, includes 0.1 M KCl as a supporting electrolyte. The analysis allows for the comparison of electron charge conductivity and resistivity of the modified materials against the bare GCE.

The larger semicircle associated with the bare GCE indicates higher resistivity, while $BiVO_4$ demonstrates improved electron charge conductivity relative to the bare electrode. ACBP exhibits notably high conductivity, which, when combined with the catalyst, facilitates enhanced electron transfer. This evidence supports the conclusion that the synthesized composite possesses superior charge conductivity and exhibits significantly higher electrocatalytic activity compared to the bare GCE. Consequently, the composite-modified GCE is utilized for further evaluations of electrocatalytic performance. The results were analyzed using the Randles equivalent circuit model (inset of Fig. 5(a)).

The EIS curve comprises two primary regions: a semicircular region at high frequencies representing the charge transfer process at the electrode–electrolyte interface, and a linear region corresponding to the inherent capacitance of the electrodes. The EIS data were fitted to an equivalent circuit model, where the diameter of the semicircle in the high-frequency

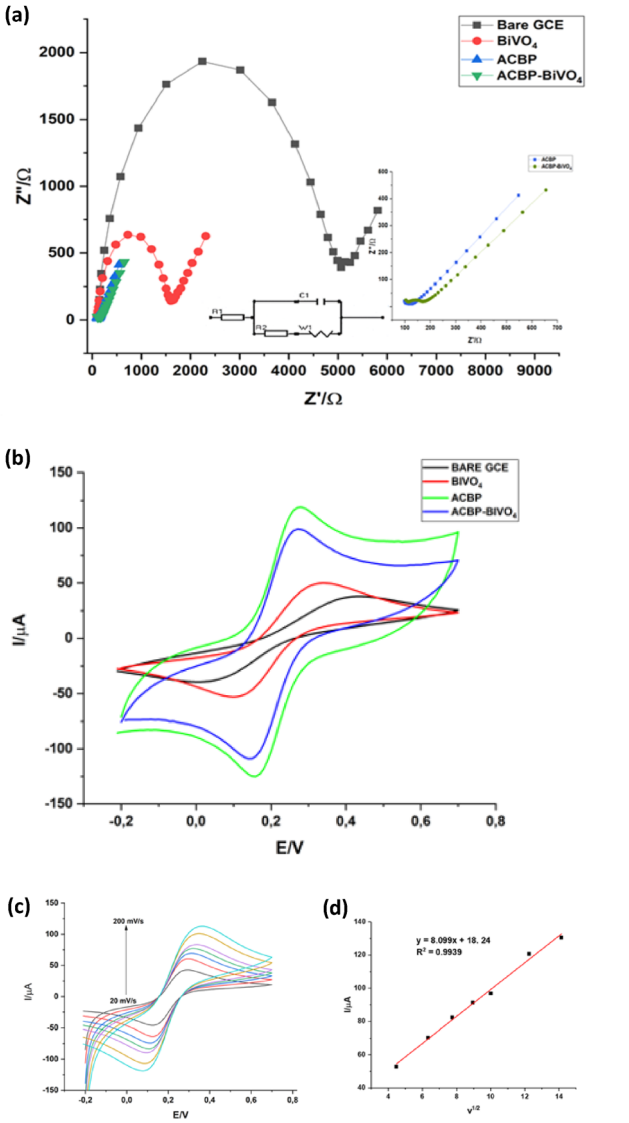

Fig. 5 Presents several analyses: (a) a Nyquist plot comparing the bare glassy carbon electrode (GCE) with the GCE modified by $BiVO_4$, ACBP, and both ACBP and $BiVO_4$, all tested in a 0.1 M KCl solution containing 5 mM $[Fe(CN)_6]^{3-/4-}$ at a scan rate of 0.05 V s^{-1}; (b) cyclic voltammetry (CV) results for the same electrodes under identical conditions; and (c, d) a scan rate study specifically for the GCE/$BiVO_4$, GCE/ACBP, and GCE/ACBP–$BiVO_4$ configurations, again in the presence of the 0.1 M KCl solution with 5 mM $[Fe(CN)_6]^{3-/4-}$.

domain provided the value of the charge transfer resistance (R_{ct}). The charge transfer resistance values were determined from the semicircular portions of the EIS curves, with R_{ct} being ascertained from the diameter of the semicircle across the higher to lower frequency regions.

The electrical conductivity of various electrode materials was assessed using cyclic voltammetry (CV). The analysis was conducted in the presence of 5 mM $Fe(CN)_6^{3-/4-}$ with 0.1 M KCl serving as the electrolyte. The ACBP-modified glassy carbon electrode (GCE) exhibited superior electron charge conductivity, characterized by a high current response and low peak potential, in comparison to the bare GCE, $BiVO_4$/GCE, and

ACBP–$BiVO_4$/GCE, as illustrated in Fig. 5(b). Although the ACBP–$BiVO_4$ composite demonstrated a reduced electroactive surface area relative to ACBP, this reduction can be attributed to the closure of some pores during the incorporation of $BiVO_4$ into the composite structure. This decrease in surface area is offset by an increase in the sensitivity of the composite.

Furthermore, the redox peak current for $BiVO_4$/GCE was lower than that of the bare GCE, ACBP/GCE, and ACBP–$BiVO_4$/GCE, which can be rationalized by the insulating nature of the oxygen functionalities present in $BiVO_4$, impeding the diffusion of $Fe(CN)_6^{3-/4-}$ and leading to increased internal resistance. The peak-to-peak separations for the bare GCE, $BiVO_4$/GCE, ACBP/GCE, and ACBP–$BiVO_4$/GCE were measured at 440, 340, 280, and 270 mV, respectively. The charge transfer resistance (R_{ct}) values were calculated as 4337, 1386, 2906, and 3605 Ω for the bare GCE, ACBP/GCE, $BiVO_4$/GCE, and ACBP–$BiVO_4$/GCE, respectively. This indicates that the composite exhibits a favourable orientation of heteroatoms within the carbon lattice. In summary, the CV analysis of ACBP–$BiVO_4$ revealed a high peak current, reflecting an enhanced electroactive surface area. Additionally, electrochemical impedance spectroscopy (EIS) studies, as shown in Fig. 5(a), indicated that ACBP–$BiVO_4$ displayed lower resistance compared to both the bare GCE and other modified electrodes, signifying reduced resistance, high electron conductivity, and rapid electron transfer kinetics to the redox probe.

As shown in Fig. 5(c), the impact of scan rate on the ACBP–$BiVO_4$/GCE was also assessed. As shown in Fig. 5(d), the results showed that the anodic and cathodic peak currents rose linearly with the scan rate, ranging from 20 to 200 mV s^{-1}.

$$i_{pa} = (2.69 \times 10^5) n^{\frac{3}{2}} A C D^{\frac{1}{2}} v^{\frac{1}{2}} \quad (1)$$

where v is the scan rate, $D = 7.6 \times 10^{-6}$ cm^2 s^{-1}, i_p is equal to i_{pa}, n is the number of electrons, and C is the concentration of the ferricyanide probe molecule in the solution (mol cm^{-3}). The EA was estimated from the oxidation peak current. The estimated electroactive surface area (EA) values for the bare glassy carbon electrode (GCE), activated carbon black/polyaniline (ACBP), bismuth vanadate ($BiVO_4$), and ACBP–$BiVO_4$ modified GCE were determined to be 0.01825, 0.1648, 0.02259, and 0.3089, respectively. Among these electrodes, the ACBP–$BiVO_4$ modified GCE demonstrates a significantly enhanced electroactive surface area, indicating its superior electrical conductivity. The sensor's efficacy relies on the electrocatalytic activity of the working electrode, which is enhanced by the electrode surface modification. The use of $BiVO_4$, which exhibits multiple oxidation states, provides numerous active sites for interaction with ciprofloxacin, enhancing the electronic structure of its products. $BiVO_4$ enables rapid electron transport for the electrochemical sensor and provides superior cycling stability. The glassy carbon electrodes (GCEs) are activated through cyclic voltammetry, which helps in cleaning and preparing the electrode surface for reversible reactions.

Electrocatalytic activity of the modified electrodes

The electrochemical characterization of the synthesized materials was conducted utilizing differential pulse voltammetry (DPV).

Influence of different pH

The electrochemical response of CPX depends on the pH of the solution. Hence, we examined the electrocatalytic behaviour of g modified ACBP–$BiVO_4$ electrode towards CPX oxidation using differential pulse voltammetry (DPV) method at pH ranges from 2 to 14 in 1 μM CPX as shown in Fig. 6(a)–(c). The oxidation peak current of CPX changed from −0.100 to −0.355 with the increase in pH range from 2 to 10 and the maximum potential oxidation potential of CPX was reached from pH 12–14 E_p = −0.03957 pH-0.03559; R^2 = 0.9947. The negative shift observed for the oxidation potential arose from a decline in available protons in the system as the pH value increased. This occurrence alters the interaction between the deprotonated CPX, thus influencing the oxidation behaviour of CPX. The slope of 39.67 mV per pH (pH *vs.* *E*, Fig. 7b). The fact that this result is nearly identical to the expected value of 59 mV per pH suggests that the same protons and electrons are involved in the electrochemical process. Scheme 4 provides a summary of the electrochemical reaction process for CPX oxidation at GCE/ACBP–$BiVO_4$. The electrode reaction, which has an apparent pK_a value of roughly 12, is thought to be connected to the protonation site based on the location of the break in the *E vs.* pH plot. In Scheme 4, the structure of CPX displays a secondary

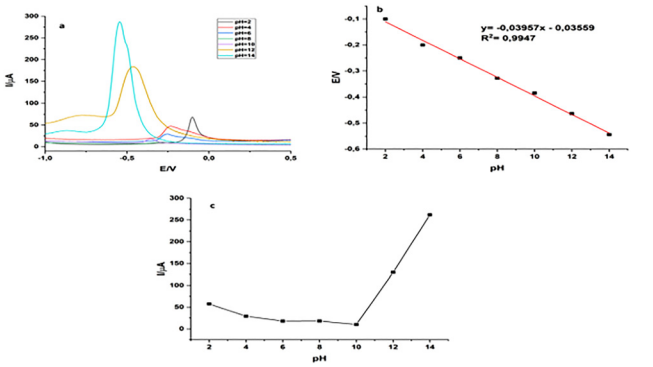

Fig. 6 (a)–(c) DPV response of pH 2,4,6,8,10 and 12 on GCE\ACBP–$BiVO_4$ in PBS and DPV parameters: E_{start} = −1.6 V; E_{end} = 1.3 V; pulse amplitude = 50.0 mV; E_{step}= 4, pulse time = 10 ms, scanrate = 100 mV s^{-1}, equilibrium time =5 s.

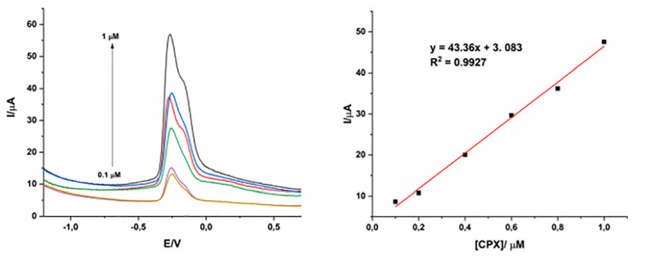

Fig. 7 (a) DPV response of 0.1, 0.2, 0.4, 0.6, 0.8 and 1 mM CPX on GCE\ACBP–$BiVO_4$ in PBS and DPV parameters: E_{start} = −1.6 V; E_{end} = 1.3 V; pulse amplitude = 50.0 mV; E_{step}= 4, pulse time = 10 ms, scanrate = 100 mV s^{-1}, equilibrium time = 5 s. Linear plot of peak current response *vs.* *C* [CPX].

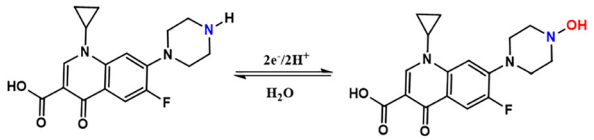

Scheme 4 Mechanism for the electro-oxidation of CPX.

amine group that functions as a basic center by acting as a donor for non-bonding electrons. Consequently, it is believed that CPX oxidizes at the –NH group to generate –N–OH.[12] The electrochemical mechanism for ciprofloxacin (CPX) detection using the ACBP/$BiVO_4$ nanocomposite involves several key steps. Initially, CPX is adsorbed onto the modified electrode through interactions with ACBP and $BiVO_4$ The electrochemical oxidation of CPX then occurs, primarily at the piperazinyl amino group, resulting in the formation of CPX^{2+} along with the release of electrons and protons, as shown in the equation:

$$CPX \rightarrow CPX^{2+} + 2e + 2H^+$$

Bismuth vanadate ($BiVO_4$) plays a crucial role in facilitating electron transfer by undergoing redox reactions:

$$BiVO_4 + e^- \rightleftharpoons BiVO_4$$

ACBP enhances this process by providing a high surface area for CPX adsorption and improving electron transport due to its conductive nature. The overall synergistic effect leads to efficient CPX detection, summarized as:

$$CPX + BiVO_4 \rightarrow CPX^{2+} + BiVO_4^- + 2H^+ \quad BiVO_4^- \rightarrow BiVO_4 + e^-$$

Differential pulse voltammetry analysis (DPV)

The differential pulse voltammetry (DPV) technique was employed to analyze the oxidation of ciprofloxacin (CPX) under optimized experimental conditions. As shown in Fig. 7(a), the DPV response for the ACBP–$BiVO_4$ modified glassy carbon electrode (GCE) was assessed for varying concentrations of CPX from 0.1 to 1 μM in a 0.1 M phosphate buffer solution (PBS) at pH 7. The anodic peak potential (i_{pa}) associated with the oxidation of CPX was recorded at 0.25 V, with the peak current demonstrating a direct proportionality to the CPX concentration. Furthermore, the peak current exhibited a linear increase with higher concentrations of TCP, as illustrated in Fig. 6(a). The resulting linear regression equation was i_{pa} (μA) = 43.36x + 3.083, with a correlation coefficient (R^2) of 0.9927, where x denotes the concentration of CPX. The calculated sensitivity for CPX was determined to be 0.4265 μA mM^{-1} cm^{-2}, this is explained by the modified GCE's reduced charge transfer resistance and the catalytic qualities of the modified electrode's increased electron transfer efficiency between CPX and the modified electrode.

The following formula can be used to determine the limit of detection:

$$LOD = \frac{3SD}{m} \quad \text{and} \quad LOQ = \frac{10SD}{m}$$

The slope value from the linear calibration plot is indicated by m, and SD stands for the standard deviation of blank (S/N = 3). The results of the calculation showed that the LOQ was 0.4265 μM and the LOD of ACBP–$BiVO_4$/GCE was 0.1279 μM. The analytical parameters from this work and those published in the literature are contrasted in Table 1. The results show that the GCE/ACBP–$BiVO_4$ system has a high degree of sensitivity and show results that are similar to what other researchers have found.

Selectivity, stability, repeatability and reproducibility of the modified GCE/ACBP–$BiVO_4$

The stability of the ACBP–$BiVO_4$ electrode was evaluated through the detection of ciprofloxacin (CPX) over four consecutive cycles. As illustrated in Fig. 8(a), the removal efficiency of CPX exhibited a slight decline but remained above 90% after 30 minutes across all four cycles, with an overall CPX removal efficiency of approximately 59.32% after the fourth cycle, demonstrating the excellent stability of the ACBP–$BiVO_4$ electrode for repeated use. The repeatability and reproducibility of the modified glassy carbon electrode (GCE) were assessed by preparing five individual electrodes, each tested for CPX detection in 0.1 M phosphate buffer solution (PBS) with the addition of 1 μM CPX. Fig. 8(b) indicates satisfactory reproducibility, with a relative standard deviation (RSD) of 0.382 μM, confirming the reliable performance of the ACBP–$BiVO_4$ modified GCE for CPX detection. Additionally, the CPX sensor maintained approximately 90% of its initial peak current after 30 days in a 0.01 M PBS solution at pH 12, indicating good storage stability, as shown in Fig. 8(c). Interference studies conducted in the

Table 1 Comparison of the results of proposed sensor (ACBP–$BiVO_4$/GCE) with previously reported CPX sensor

Modified electrodes	pH	Linear range	LOD	Ref.
Au–PAMAM/rGO	—	1 μM–1 nM	1 nM	2
MWCNT/DNA/GCE	7.0	96.0–223 μg mL^{-1}	0.33 μg mL^{-1}	42
Ag-β-CD/GCE	7.0	0.1 nM to 50 nM	0.028 nM	1
Graphene-modified GCE	1.0	1.0×10^{-7} to 1.0×10^{-5} mol L^{-1}	5.9×10^{-8} mol L^{-1}	43
TiO_2/Nafion/CMK-3, TiO_2/AuNPs/Nafion/CMK-3	6.0	1 to 10 μM	0.108 μM	44
rGO/PPR/GCE	5.5	0.002–0.05 μM	2 nM	45
AuNP/CHI/SPE	5.5	0.1–150 μM	0.001 μM	46
Cip-Tob	9.5	0.007 mM to 1 mM	0.25 mM	4
ACBP–$BiVO_4$/GCE	12	0.1–1 μM	0.1279 μM	This work

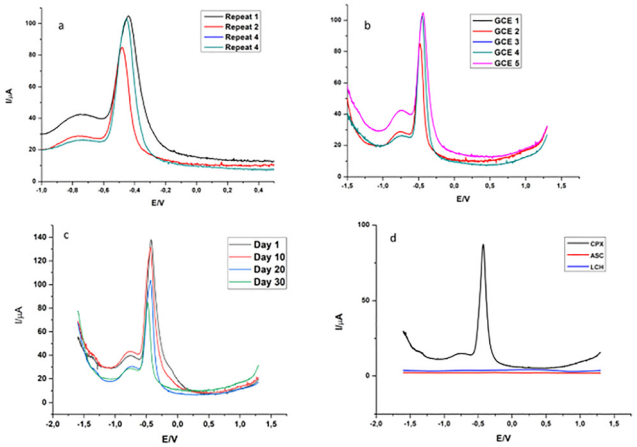

Fig. 8 DPV response of 1 mM CPX on GCE\ACBP–$BiVO_4$ in PBS (a) repeatability for 4 successive measurements, (b) reproducibility and (c) long-term storage stability, (d) interference studies on 1 mM CPX on GCE\ACBP–$BiVO_4$ in PBS DPV parameters: E_{start} = −1.6 V; E_{end} = 1.3 V; pulse amplitude = 50.0 mV; E_{step} = 4, pulse time = 10 ms, scanrate = 100 mV s^{-1}, equilibrium time = 5 s.

presence of ascorbic acid (ASC) and L-cysteine hydrochloride (LCH) demonstrated that neither interfered with the detection of CPX, suggesting that the ACBP–$BiVO_4$/GCE exhibits selectivity specifically for CPX, thereby validating its suitability as a modifier for CPX detection, as depicted in Fig. 8(d).

Real sample analysis

The ACBP–$BiVO_4$ modified glassy carbon electrode (GCE) was utilized for the detection of ciprofloxacin (CPX) in real water samples, with the sample preparation detailed in Section 2.8. The wastewater sample was spiked with a known concentration of CPX and analyzed at various concentrations using the differential pulse voltammetry (DPV) technique with a scan rate of 100 mV s^{-1}. The results of these analyses are presented in Table 2. The synthesized composite electrode demonstrated effectiveness for real-time applications, yielding satisfactory results as reported in Table 2.

To assess the significance of CPX concentrations in tablet samples at four distinct levels, a *t*-test was performed, utilizing the null hypothesis based on results obtained from the UV-vis spectrophotometric method. The computed *t* value was 0.6510, compared to a critical *t* value of 2.264. Since the calculated *t* value was lower than the critical value at a 95% confidence level with degrees of freedom of $n - 1$, it indicates that the proposed method is appropriate for quantifying CPX concentrations. These findings suggest that it is feasible to analyze CPX levels even in the presence of significant interferences using this approach. Furthermore, as indicated in Table 2, the electrochemical sensing results for CPX in analyses of real samples were consistent with those obtained *via* the UV-vis method.

Table 2 The detection of CPX in the treated water sample using ACBP–$BiVO_4$ modified GCE

		Detected (μM)		
Sample	Spiked (μM)	DPV	UV-Vis	Recovery (%)
Treated water	0	0.41	0.40	99.31
	10	0.63	0.60	99.38
	20	0.88	0.90	99.40
	30	1.01	1.0	99.62
	40	1.02	1.3	99.43
	50	1.11	1.4	99.74

Conclusions

This study successfully developed and validated a novel electrochemical sensor based on an ACBP–$BiVO_4$ nanocomposite for the rapid and cost-effective detection of ciprofloxacin (CPX) in environmental samples. The synergistic combination of activated carbon derived from banana peels (ACBP) and bismuth vanadate ($BiVO_4$) resulted in a sensor with enhanced surface area, sensitivity, and electrochemical performance. The modified GCE/ACBP–$BiVO_4$ electrode demonstrated excellent CPX detection capabilities within a linear range of 0.1–1 μM, a correlation coefficient of 0.9927, and a recovery rate of 99 ± 6% in spiked wastewater samples. The determined limits of detection (LOD) and quantification (LOQ) were 0.1279 μM and 0.4265 μM, respectively, highlighting the sensor's sensitivity. This work demonstrates the potential of utilizing agricultural waste and nanomaterials to create a sustainable and efficient technology for environmental monitoring, offering a promising alternative to traditional, more complex methods for antibiotic detection. The ACBP/$BiVO_4$ nanocomposite sensor addresses the pressing need for low-cost, feasible, and time-saving methods for detecting CPX in water sources, contributing to improved environmental safety and public health.

Conflicts of interest

There are no conflicts to declare.

Data availability

Data will be made available on request.

Acknowledgements

We would like to acknowledge the Faculty of Science, University of Johannesburg, Centre for Nanomaterials Science Research, University of Johannesburg, GES, University of Johannesburg and National Research Foundation, South Africa.

References

1 A. A. S. Gill, *et al.*, One-pot synthesis of β-cyclodextrin modified silver nanoparticles for highly sensitive detection of ciprofloxacin, *J. Pharm. Biomed. Anal.*, 2021, **203**, 114219, DOI: 10.1016/j.jpba.2021.114219.

2 M. Mahmoudpour, H. Kholafazad-kordasht, J. E. Nazhad Dolatabadi, M. Hasanzadeh, A. H. Rad and M. Torbati, Sensitive aptasensing of ciprofloxacin residues in raw milk samples using reduced graphene oxide and nanogold-functionalized poly(amidoamine) dendrimer: an innovative apta-platform towards electroanalysis of antibiotics, *Anal. Chim. Acta*, 2021, **1174**, 338736, DOI: 10.1016/j.aca.2021.338736.

3 G. Divyapriya, J. Mohanalakshmi, V. Keshav and I. M. Nambi, Electro-enhanced adsorptive removal of cipro fl oxacin from aqueous solution on graphite felt, *J. Environ. Chem. Eng.*, 2020, **8**(5), 104299, DOI: 10.1016/j.jece.2020.104299.

4 R. Islam, V. Singh, D. Ammeter, F. Schweizer and S. Kuss, Electrochemical characterization of the antibiotic hybrid ciprofloxacin-tobramycin, *Electrochem. Commun.*, 2020, **119**, 106825, DOI: 10.1016/j.elecom.2020.106825.

5 M. Harrabi, *et al.*, Analysis of multiclass antibiotic residues in urban wastewater in Tunisia, *Environ. Nanotechnology, Monit. Manage.*, 2018, **10**, 163–170, DOI: 10.1016/j.enmm.2018.05.006.

6 X. Yi, C. Lin, E. Jie, L. Ong, M. Wang and Z. Zhou, Occurrence and distribution of trace levels of antibiotics in surface waters and soils driven by non-point source pollution and anthropogenic pressure, *Chemosphere*, 2019, **216**, 213–223, DOI: 10.1016/j.chemosphere.2018.10.087.

7 M. Pant and S. Palsule, Synergistic effects of Areca and pineapple fiber reinforcements for sustainability of functionalized polypropylene hybrid composites, *Ind. Crops Products*, 2025, **223**, 120253, DOI: 10.1016/j.indcrop.2024.120253.

8 S. Cotton, M. P. Mchugh, M. Etherson, J. Shepherd and K. E. Templeton, Evaluation of the molecular detection of ciprofloxacin resistance in Neisseria gonorrhoeae by the ResistancePlus GC assay (SpeeDx), *Diagnostic Microbiol. Infect. Dis.*, 2021, **99**(4), 115262, DOI: 10.1016/j.diagmicrobio.2020.115262.

9 S. V. Kergaravat, N. Romero, L. Regaldo, G. R. Castro, A. María and R. Hern, Simultaneous electrochemical detection of ciprofloxacin and Ag(I) in a silver nanoparticle dissolution: application to ecotoxicological acute studies, *Microchem. J.*, 2021, **162**, 105832, DOI: 10.1016/j.microc.2020.105832.

10 W. D. Adane, B. S. Chandravashi and M. Tessema, A simple, ultrasensitive and cost-effective electrochemical sensor for the determination of ciprofloxacin in various types of samples, *Sens. Biosens. Res.*, 2023, **39**, 100547, DOI: 10.1016/j.sbsr.2022.100547.

11 Y. He, *et al.*, Evaluation of attenuation of pharmaceuticals, toxic potency, and antibiotic resistance genes in constructed wetlands treating wastewater effluents, *Sci. Total Environ.*, 2018, **631–632**, 1572–1581, DOI: 10.1016/j.scitotenv.2018.03.083.

12 S. Bano, A. S. Ganie, R. I. A. Khan, S. Sultana, M. Z. Khan and S. Sabir, Designing and application of PPy/Bi_2MoO_6/chitosan nanocomposites for electrochemical detection of ciprofloxacin and benzene and evaluation of hydrogen evolution reaction, *Surf. Interfaces*, 2022, **29**, 101786, DOI: 10.1016/j.surfin.2022.101786.

13 F. Li, Y. Wu, D. Chen, Y. Guo, X. Wang and X. Sun, Sensitive dual-labeled electrochemical aptasensor for simultaneous detection of multi-antibiotics in milk, *Int. J. Hydrogen Energy*, 2021, **46**(45), 23301–23309, DOI: 10.1016/j.ijhydene.2021.04.007.

14 A. K. Yadav, D. Verma, G. B. V. S. Lakshmi, S. Eremin and P. R. Solanki, Fabrication of label-free and ultrasensitive electrochemical immunosensor based on molybdenum disulfide nanoparticles modified disposable ITO: an analytical platform for antibiotic detection in food samples, *Food Chem.*, 2021, **363**, 130245, DOI: 10.1016/j.foodchem.2021.130245.

15 S. A. R. Alavi-tabari, M. A. Khalilzadeh and H. Karimi-maleh, Simultaneous determination of doxorubicin and dasatinib as two breast anticancer drugs uses an ampli fi ed sensor with ionic liquid and ZnO nanoparticle, *J. Electroanal. Chem.*, 2018, **811**, 84–88, DOI: 10.1016/j.jelechem.2018.01.034.

16 H. Fu, X. Yang, X. An, W. Fan, X. Jiang and A. Yu, Experimental and theoretical studies of V_2O_5@TiO_2 core–shell hybrid composites with high gas sensing performance towards ammonia, *Sens. Actuators, B*, 2017, **252**, 103–115, DOI: 10.1016/j.snb.2017.05.027.

17 S. Singha and K. H. Ahn, Detection of ciprofloxacin in urine through sensitized lanthanide luminescence, *Sensors*, 2016, **16**(12), 2065, DOI: 10.3390/s16122065.

18 R. D. Crapnell, P. S. Adarakatti and C. E. Banks, Electroanalytical overview: the measurement of ciprofloxacin, *Sens. Diagn.*, 2023, **3**(1), 40–58, DOI: 10.1039/d3sd00129f.

19 R. D. Crapnell and C. E. Banks, Electroanalytical overview: the measurement of ciprofloxacin, *Sens. Diagn.*, 2024, 40–58, DOI: 10.1039/d3sd00129f.

20 W. Lai, *et al.*, $BiVO_4$ prepared by the sol–gel doped on graphite felt cathode for ciprofloxacin degradation and mechanism in solar-photo-electro-Fenton, *J. Hazard. Mater.*, 2021, **408**, 124621, DOI: 10.1016/j.jhazmat.2020.124621.

21 R. Srinivasan, E. Elaiyappillai, S. Anandaraj, B. kumar Duvaragan and P. M. Johnson, Study on the electrochemical behavior of $BiVO_4$/PANI composite as a high performance supercapacitor material with excellent cyclic stability, *J. Electroanal. Chem.*, 2020, **861**, 113972, DOI: 10.1016/j.jelechem.2020.113972.

22 W. D. Adane, B. S. Chandravanshi, N. Getachew and M. Tessema, A cutting-edge electrochemical sensing platform for the simultaneous determination of the residues of antimicrobial drugs, rifampicin and norfloxacin, in water samples, *Anal. Chim. Acta*, 2024, **1312**, 342746, DOI: 10.1016/j.aca.2024.342746.

23 Q. H. Zhang, W. N. Yang, H. H. Ngo, W. S. Guo, P. K. Jin, M. Dzakpasu, S. J. Yang, Q. Wang, X. C. Wang and D. Ao, Behavior of NiO–MnO 2/MWCNT composites for use in a supercapacitor, *Environ. Int*, 2016, **92–93**, 11–22, DOI: 10.1016/j.envint.2016.03.024.

24 D. Prabu, B. Thirumalraj and S. Chen, Facile synthesis of hierarchically nanostructured bismuth vanadate: an efficient photocatalyst for degradation and detection of hexavalent chromium, *J. Hazard. Mater.*, 2019, **367**, 647–657, DOI: 10.1016/j.jhazmat.2019.01.017.

25 L. DengJ. Liu, Z. Ma, G. Fan and Z-h. Liu, Free-standing graphene/bismuth vanadate monolith composite as a

binder-free electrode for symmetrical supercapacitors, *RSC Adv.*, 2018, 24796–24804, DOI: 10.1039/c8ra04200d.

26 Y. Sun, Research on Detection of Sterol Doping in Sports by Electrochemical Sensors: A Review, *J. Anal. Methods Chem.*, 2022, DOI: 10.1155/2022/3394079.

27 S. Saisree, C. J. Aleena and A. Chandran, Paper-based printed electrochemical sensor for the detection of hydroxymethyl furaldehyde in foods using nitrogen and sulphur co-doped graphene quantum dots, *J. Electroanal. Chem.*, 2025, **985**, 119080.

28 L. Qiao, *et al.*, Designing a Stable g-C_3N_4/$BiVO_4$-Based Photoelectrochemical Aptasensor for Tetracycline Determination, *Toxics*, 2023, **11**(1), 1–10, DOI: 10.3390/toxics11010017.

29 S. Menon, M. R. Mathew, S. Sam, K. Keerthi and K. G. Kumar, COVID-19 resource centre with free information in English and Mandarin on the novel coronavirus COVID-19. The COVID-19 resource centre is hosted on Elsevier Connect, the company's public news and information, 2020.

30 M. Ramzan, A. S. Alqarni, K. Ahmad, A. G. Al-Sehemi, A. M. A. Henaish, M. Aslam, M. J. Khan and M. Saleem, Hydrothermally fabricated $MoTe_2$/rGO as a proficient electrocatalyst for robust oxygen evolution reaction, *Diamond Related Mater.*, 2024, **148**, 111364, DOI: 10.1016/j.diamond.2024.111364.

31 N. M. Sulthana, K. Ganesan and P. K. Ajikumar, Enhanced sensitivity of partial O-terminated H-diamond for H_2S detection at room temperature, *Diamond Related Mater.*, 2023, **140**, 110568, DOI: 10.1016/j.diamond.2023.110568.

32 A. Hamid, Z. Rahmawati, M. Abdullah, T. E. Purbaningtyas, F. Rohmah and I. D. Febriana, The Influence of NaOH Activator Concentration on the Synthesis of Activated Carbon from Banana Peel for Pb(II) Adsorption, *Eksakta Berk. Ilm. Bid. MIPA*, 2022, **23**(03), 158–166, DOI: 10.24036/eksakta/vol23-iss03/323.

33 T. Van Thuan, B. Thi, P. Quynh, T. Duy and V. T. Thanh, Response surface methodology approach for optimization of Cu^{2+}, Ni^{2+} and Pb^{2+} adsorption using KOH-activated carbon from banana peel, *Surf. Interfaces*, 2017, **6**, 209–217, DOI: 10.1016/j.surfin.2016.10.007.

34 A. P. Nowak, K. Trzciński, M. Szkoda, J. Karczewski, M. Gazda and A. Lisowska-Oleksiak, A negative effect of carbon phase on specific capacity of electrode material consisted of nanosized bismuth vanadate embedded in carbonaceous matrix, *Synth. Met.*, 2019, **257**, 116168, DOI: 10.1016/j.synthmet.2019.116168.

35 L. Chen, D. Meng, X. Wu, J. Wang, Y. Wang and Y. Liang, Shape-controlled synthesis of novel self-assembled $BiVO_4$ hierarchical structures with enhanced visible light photocatalytic performances, *Mater. Lett.*, 2016, **176**, 143–146, DOI: 10.1016/j.matlet.2016.04.112.

36 A. U. Rajapaksha, *et al.*, Pyrolysis condition affected sulfamethazine sorption by tea waste biochars, *Bioresour. Technol.*, 2014, **166**, 303–308, DOI: 10.1016/j.biortech.2014.05.029.

37 M. Yaseen, *et al.*, Oxidative desulfurization of model and real petroleum distillates using Cu or Ni impregnated banana peels derived activated carbon–NaClO catalyst–oxidant system, *Chem. Eng. Res. Des.*, 2022, **179**, 107–118, DOI: 10.1016/j.cherd.2022.01.018.

38 J. Y. Yusuf, H. Soleimani, L. K. Chuan, Y. K. Sanusi and L. L. Adebayo, Physicochemical properties and microwave absorption performance of Co_3O_4 and banana peel-derived porous activated carbon composite at X-band frequency, *J. Alloys Compd.*, 2021, **888**, 161474, DOI: 10.1016/j.jallcom.2021.161474.

39 Y. Y. Lin, H. T. Chi, J. H. Lin, F. H. Chen, C. C. Chen and C. S. Lu, Eight crystalline phases of bismuth vanadate by controllable hydrothermal synthesis exhibiting visible-light-driven photocatalytic activity, *Mol. Catal.*, 2021, **506**, 111547, DOI: 10.1016/j.mcat.2021.111547.

40 T. R. A. Thara, P. P. Rao, A. K. V. Raj and T. S. Sreena, New series of brilliant yellow colorants in rare earth doped scheelite type oxides, $(LiRE)_{1/2}WO_4$–$BiVO_4$ for cool roof applications, *Sol. Energy Mater. Sol. Cells*, 2019, **200**, 110015, DOI: 10.1016/j.solmat.2019.110015.

41 I. Benisti, R. Nandi, N. Amdursky and Y. Paz, Nanoseconds-resolved transient FTIR spectroscopy as a tool for studying the photocatalytic behavior of various types of bismuth vanadate, *Appl. Catal., B*, 2020, **278**, 119351, DOI: 10.1016/j.apcatb.2020.119351.

42 L. Fotouhi, Z. Atoofi and M. M. Heravi, Interaction of ciprofloxacin with DNA studied by spectroscopy and voltammetry at MWCNT/DNA modified glassy carbon electrode, *Talanta*, 2013, **103**, 194–200, DOI: 10.1016/j.talanta.2012.10.032.

43 J. Shan, Y. Liu, R. Li, C. Wu, L. Zhu and J. Zhang, Indirect electrochemical determination of ciprofloxacin by anodic stripping voltammetry of Cd(II) on graphene-modified electrode, *J. Electroanal. Chem.*, 2015, **738**, 123–129, DOI: 10.1016/j.jelechem.2014.11.031.

44 A. Pollap, K. Baran, N. Kuszewska and J. Kochana, Electrochemical sensing of ciprofloxacin and paracetamol in environmental water using titanium sol based sensor, *J. Electroanal. Chem.*, 2020, **878**, 114574, DOI: 10.1016/j.jelechem.2020.114574.

45 R. Chauhan, A. A. S. Gill, Z. Nate and R. Karpoormath, Highly selective electrochemical detection of ciprofloxacin using reduced graphene oxide/poly(phenol red) modified glassy carbon electrode, *J. Electroanal. Chem.*, 2020, **871**, 114254, DOI: 10.1016/j.jelechem.2020.114254.

46 K. R. Reddy, P. K. Brahman and L. Suresh, Fabrication of high performance disposable screen printed electrochemical sensor for ciprofloxacin sensing in biological samples, *Meas. J. Int. Meas. Confed.*, 2018, **127**, 175–186, DOI: 10.1016/j.measurement.2018.05.078.